Experimental study of lateral load behavior of Hshaped precast reinforced concrete shear walls with bolted steel connections

Experimental study of lateral load behavior of H-shaped precast reinforced concrete shear walls with bolted steel connections

Jian Sun[1,*], Hongxing Qiu[1], Yong Lu[2], Hongbo Jiang[1]

[1] Key Laboratory of Concrete and Prestressed Concrete Structures of Ministry of Education, School of Civil Engineering, Southeast University, Nanjing, China;

[2] Institute for Infrastructure and Environment, School of Engineering, The University of Edinburgh, Edinburgh, UK

Abstract. This paper presents an experimental study of H-shaped precast reinforced concrete (RC) shear walls involving vertical connections under combined vertical and lateral loading. The H-wall is composed of two prefabricated flange wall panels, one prefabricated web wall panel, and vertical bolted steel connections between the flange and web panels. The assembling of the H-wall is completely dry without any in-situ casting. Three H-wall specimens were constructed and tested to investigate the mechanical behavior and seismic performance of them. The lateral load bearing capacity, ductility, energy dissipation, lateral stiffness, strain in the connecting steel frame (CSF), and sliding within the bolted steel connections are presented and discussed to evaluate the effectiveness of the vertical connections. The ultimate shear-resistance mechanism of the precast H-wall assembly is also analyzed. The H-wall assemblies generally possess high load bearing capacity, favorable ductility and good energy-dissipating capacity. The thickness of the steel plates in the CSF affect the lateral stiffness and the ultimate load bearing capacity of the H-walls. Furthermore, the encasing steel plates (ESP) for the web wall panel not only helps transfer the

*Correspondence to: Jian Sun, Key Laboratory of Concrete and Prestressed Concrete Structures of Ministry of Education, School of Civil Engineering, Southeast University, Nanjing 211189, China.

Email: sunjian@seu.edu.cn

stress in the wall steel bars, but also confines the concrete resulting in improved ductility.

Keywords: precast shear wall; bolted steel connection; ductility; load bearing capacity; energy dissipation; high strength bolt

1. Introduction and background

Precast reinforced concrete (RC) construction is widely adopted around the world. It allows mass production of standard components in a factory environment, thus leading to considerable reduction of the construction time and labour cost, and better quality control [1]. Precast RC structures with earthquake-resistant connections and detailing are also popular in seismic regions [2, 3].

Comparing with other precast components, precast RC shear walls remain to be a challenging subject and this is primarily because of the high demand on the connections to make an assembled shear wall work effectively. Shear walls are key structural components to resist lateral seismic loading in high-rise buildings [4, 5]. Due to the need of maintaining high lateral stiffness and resistance, precast RC shear wall poses particular challenges to the assembling techniques. Various forms of prefabricated RC shear walls have been investigated in the literature, and most of these studies involved some degree of “wet” assembling process. Research into the use of the potentially more favourable “dry”-only methods is still limited.

The unbonded post-tensioned (UPT) precast concrete wall system is a representative type of prefabricated shear walls with dry connections, which has been subject to a series of studies in the literature [6-9]. In this system, the upper and lower post-tensioned precast wall panels are normally assembled across horizontal joints at the floor levels using UPT steel, while vertical joints between the adjacent wall panels generally use ductile connectors to transfer the vertical shear force and dissipate energy under seismic loading. Further studies [10-12] adopted a combination of mild steel and

high-strength UPT steel to enhance the energy-dissipating capacity of the UPT walls. However, thicker walls are generally required to cope with the high compressive force resulting from the vertical post-tensioning in the UPT precast concrete wall system, and special confining reinforcement such as spiral reinforcement may also be required at the edges of the wall.

Precast concrete walls can also be joined together using mechanical bolted connections [13-15]. Such connections usually involve steel inserts embedded in the concrete wall by stud-welded anchor bars. During erection two such inserts are firstly held in place adjacent to each, and then a connecting plate is bolted onto the embedded inserts to complete the connection. Bora *et al.* [16] used a slotted-bolted (SB) connection to join hollow-core panel with floor slabs to form a precast concrete shear wall system, especially for low-rise buildings. Due to the elastic-plastic response of the SB connection resulting from a certain amount of allowable slippage between the plates under a seismic force, the connection could provide the wall panel with ductility and load-limiting control, as well as with high energy-dissipating capacity. Lim *et al.* [17] developed a precast concrete T-shaped wall system, which consists of bolt-type connection between the upper and lower precast concrete walls and emulated cast-in-place joints between the flange-wall and web-wall.

An innovative precast RC shear wall system using bolted steel connections has been under development by the authors and their co-workers [18-20]. Depending on the wall configuration, the connections are divided into horizontal and vertical joints. As studied previously [18], horizontal joints utilizes horizontal steel connector and high-strength bolts to assemble the adjacent upper and lower shear wall panels and floor slabs to form an integrated lateral load-resisting structural system, serving to transfer both gravity loads and horizontal loads to the base foundation. Vertical joints, on the other hand, connect the vertical sides of adjoining wall panels and primarily act as vertical shear links to

ensure the composite effect of the assembled wall system.

As a novel and developing system, the proposed precast shear wall not only possesses the general advantages aforementioned when compared with cast-in-situ monolithic concrete shear wall, but also is characterized by some particular merits due to the introduction of bolted connection. As is well known, it is the bolted connection together with welding connection that enable the high-efficiency in the construction of steel structures. Similarly, in the proposed precast reinforced concrete shear wall system the assembly efficiency is supposed to be promoted significantly as well. Now the proposed system is evolving into a steel-concrete composite structure, which demonstrates both the benefits of concrete and steel structures. Furthermore, the fire protection and corrosion protection for the steel connection in this system should be properly handled by reference to the mature measures adopted in steel structure as well as steel-concrete structure.

The results from the proof-of-concept testing studies [19], supported by the theoretical analysis [20], demonstrated that the general idea of assembling wall units through bolted steel connectors was workable in terms of both the assembling procedure and the anticipated effect. The vertical bolted connections could effectively connect the longitudinal and transverse precast wall panels and completely transfer the interactional forces between them such that the wall assembly works as a composite unit to resist the lateral seismic load. However, undesirable shear failure occurred along the H-shaped wall bottom as evidenced in the previous experiment and this limited the deformability and ductility of the assembled wall unit. To improve this situation, both the configuration and the detailed design of the vertical bolted steel connections need to be studied in a rigorous manner.

This paper presents a systematic experimental study of the H-shaped precast RC shear walls assembled by bolted steel connections, with a particular focus on improving the seismic performance

of the H-walls.

2. Experimental program

2.1. Specimen design

Prior to the experimental study presented here, a preliminary experiment on two trial precast H-wall specimens was conducted. The specimens were designed and fabricated with a length scale factor of 1/2. Fig. 1 (a) shows the assembling scheme, where CSF indicates connecting steel frame, ESP indicates encasing steel plate.

The test results exposed several issues with the initial design and the connection scheme, these include 1) both trial specimens suffered from a brittle shear failure resulting in poor seismic behavior in terms of ductility and energy dissipation capacity; 2) in the wall web, a major crack developed horizontally at its bottom, in addition to the expected inclined cracks; and 3) the bottom segment of the flange suffered from a shear similar to an RC short column. Consequently, the specimens exhibited a premature failure with shearing diagonal cracks at the flange bottom as well as a major crack across the web bottom, as shown in Fig.1 (b).

To address the above-mentioned issues, in the current study the following measures have been taken to improve the seismic performance of the precast H-walls:

1) In consideration of the concurrence of vertical and horizontal connections in a real H-shaped precast shear wall system, in the current design both the vertical and horizontal faces of the precast wall panels are encased in light steel plates which are welded together at panel corners.

2) In the preliminary specimens WV-1 and WV-2, the H-wall panels were cast together with the bottom base block and the top loading block, and only the vertical connectors were applied after the casting. In the current design, all the wall panels were cast as separate pieces, which were assembled

together and fixed onto the base and loading beams after casting. This process represents more realistically a precast wall assembling process in practice.

3) The above assembling procedure also allowed the RC loading block at the top of the test specimen and the base foundation to be prefabricated separately. This not only ensured a more realistic representation of the horizontal connection condition, but also enabled the loading block and foundation to be reused in all tests.

The overall geometry for the H-wall panels remain the same as in the previous specimens WV-1 and WV-2 with a scale factor of 1/2, as shown in Fig. 1. Three new H-shaped wall specimens were designed and fabricated, and they are labelled as WV-r1 to WV-r3. Each test specimen was composed of two precast flange wall panels and one precast web wall panel, and each flange panel can be further divided into two half-flange parts. The new configuration of H-walls is shown in Fig. 2 (a).

The differences among the three H-walls were in the connection parameters and loading mode. In specimen WV-r1, the thickness of the steel plate used in the connecting steel frame and the encasing steel plate was 6 mm, while in specimen WV-r2 it was reduced to 3 mm. Both WV-r1 and WV-r2 were subjected to monotonic lateral loading. Specimen WV-r3 was identical to WV-r1 in the design but was subjected to cyclic loading.

Other than the connections, the geometry, concrete strength, reinforcement, and layout of bolts and bolt holes were the same in all three specimens. Fig. 2 (b) shows the details of wall web, wall flange, and the connecting steel frame (CSF). The wall web was 2005 mm in height, 1220 mm in width, and 90 mm in thickness. The vertical and horizontal distributing steel bars in the web were A6@150 and A8@100, respectively, where A indicates the nominal yield strength of the steel bar is 300 MPa. Each half-flange is 2005 mm in height, 255 mm in width, and 90 mm in thickness. The

vertical and horizontal distributing steel bars in the half-flange were 6A6 and A8@100, respectively. The ends of the steel bars were welded to the inner side of encasing steel plates. The concrete was grade C35 (35 MPa compressive strength). The nominal diameter of the high strength bolt was 16 mm.

Table 1 summarizes the yield strength (f_y) and tensile strength (f_u) of steel bar and steel plate contained in CSF and ESP used in the test walls, which were obtained by testing individual coupon specimens in uniaxial tension. The strength of concrete was determined from testing standard cubes of 150×150×150 mm at approximately the same time as the test of the walls, and the average compressive strength was 37.4 MPa.

2.2. Assembling of test H-wall specimens

After the completion of all precast elements, each H-wall specimen was assembled by connecting two pairs of half-flange elements and the web panel through two CSFs and 88 high strength bolts, as shown in Fig. 3. The pre-tension force applied to each high strength bolt was determined by the nominal diameter of the bolt in accordance with relevant standards [21]. In the present case, the pre-tension force was 100 kN in the 16-mm-diameter bolt. During the assembling process, the above pre-tension force was applied to the respective bolts using a calibrated torque wrench. As for the on-site construction of full-scale walls, the assembly techniques used in conventional steel structure can be introduced to the precast shear wall system herein.

2.3. Test scheme

2.3.1 Loading procedure and test setup

All specimens were tested with a combination of axial and lateral loading. Fig. 4 shows

schematically the loading setup. The axial (vertical) force was applied through two external high-strength rods situated at the front and back of the wall using two hydraulic jacks fixed beneath the rigid platform. A constant vertical force of 500 kN was applied, giving rise to an axial compression ratio of 0.1, which represents the level of gravity load transmitted to the shear wall from the upper part of a building structure.

The horizontal (lateral) load was applied on the top loading block by a MTS actuator which was mounted on a reaction wall. The loading was applied in a force-controlled manner or displacement-controlled manner with a loading rate of 0.5 mm per minute. Based on the experiences from the preliminary experiment [19], the loading scheme for each test here was pre-scheduled as shown in Table 2.

2.3.2 Measurement scheme

The measurement scheme is illustrated in Fig. 6. The main measurements include the following:

1) Lateral load and lateral displacement at the top of the wall assembly. The lateral load was measured by a load cell attached to the MTS actuator head, and the lateral displacement was measured by a displacement transducer.

2) Strains in the CSF. 38 strain rosettes (No. 1 through No. 38) were installed on the CSF to measure its strain state and distributions.

3) Strains in steel bars. 21 strain gauges were installed on part of the vertical steel bars and 5 strain gauges on part of the horizontal steel bars.

4) Relative displacement (sliding) between CSF and ESP. This was measured by 12 linear variable displacement transducers (LVDT1 through LVDT12) fixed at key positions on the CSF.

Furthermore, an additional displacement transducer (LVDT13) was installed on the precast

concrete foundation to monitor any rigid-body translation of the whole specimen.

3. Test results and discussion

3.1. General performance and failure modes

3.1.1 Specimen WV-r1 under monotonic loading

When the lateral load reached 180 kN (and the top displacement was about 3.4 mm), specimen WV-r1 cracked horizontally at flange bottom on tensile side, as shown in Fig. 7 (a), indicating the first visible crack due to flexure. Afterwards, several horizontal flexural cracks appeared in the bottom region of the tensile flange.

When the lateral load increased to 300 kN, the first visible diagonal crack occurred in the web roughly parallel to the diagonal line of the web, as shown in Fig. 7 (b). When the lateral load increased to 320 kN, the first diagonal crack already extended to the compression corner of the web, and in the meantime a number of newly-developed inclined cracks grew in the web. The top displacement was in the range from 10 mm to 20 mm when the above inclined cracks developed.

Subsequently, the loading procedure was changed to a displacement-controlled manner. When the top displacement increased from 20 mm to 45 mm, the horizontal cracks in the tensile flange expanded through the whole flange width and depth; meanwhile, further inclined cracks formed in web and most of the existing diagonal cracks propagated to reach the compression corner of the web, as shown in Fig. 7 (b).

When the top displacement further increased from 45 mm to 75 mm, the horizontal cracks at the flange bottom region grew to 2-3 mm in width, and the concrete at the compression corner of the web continuously started to crush and spall, while inclined cracks in web stabilized. Eventually, when the

top displacement reached 75 mm, the concrete at the compression corner of the web crushed, exposing the steel bars, as shown in Fig. 7 (c). The CSF did not buckle and the bolts did not fail either. Fig. 7 (d) and (e) shows the general failure mode for specimen WV-r1.

3.1.2 Specimen WV-r2 under monotonic loading

The damage pattern and crack development in specimen WV-r2 were similar to specimen WV-r1 until the final stage of the response. At early stage of the loading procedure, the first bending crack occurred at tensile flange bottom, as shown in Fig. 8 (a), when the top displacement reached 6 mm (lateral load about 211 kN). With increasing top displacement, inclined cracks formed, expanded, and extended in the web, as shown in Fig. 8 (b). Afterwards, as the top displacement increased from 45 mm to 75 mm, both the horizontal cracks in tensile flange and the inclined cracks in web gradually developed; and concrete at the compression corner of web continuously bulged and desquamated, as shown in Fig. 8 (c).

Meanwhile, during the course of the top displacement increasing from 60 mm to 65 mm, it was noticed that local buckling failure happened to the CSF at the location about 470 mm to 615 mm above the CSF bottom, as shown in Fig. 8 (d). Eventually, concrete at the compression corner of web crushed along with the buckling and exposure of vertical steel bars. Fig. 8 (e) and (f) shows the general failure mode for specimen WV-r2.

3.1.3 Specimen WV-r3 under cyclic loading

Specimen WV-r3 was subjected to a cyclic loading with the loading scheme as shown in Fig. 5, and the lateral loading was applied in a displacement-controlled manner.

When the specimen was initially loaded to reach a top displacement of +4 mm in the positive

direction, a horizontal crack occurred at the bottom region of the tensile flange, due also to flexure. When the displacement increased to +8 mm, a diagonal crack occurred in the web. As the displacement further increased to +12 mm, more horizontal and inclined cracks developed in the tensile flange and the web, respectively. With the positive displacement reaching +35 mm, the concrete cover at the compressive flange bottom began to spall. When the displacement further increased +60 mm, concrete at both the compressive flange bottom and the compression corner of the web crushed, as shown in Fig. 9 (a). Eventually, the concrete at the compression corner of the web crushed along with buckling of the vertical steel bars; however, the connection steel frame did not buckle and the bolts did not fail either.

In the reversed direction of loading, the development of the cracks appeared to be almost symmetrical to the existing cracks from the first half cycle. Figs. 9 (b) and (c) shows the general failure mode for WV-r3.

In summary, all specimens experienced a similar pattern of response until the final stages, and the process included initial cracking of concrete at the tensile flange bottom and web; extension and expansion of concrete cracks; spalling and crushing of concrete at the compression corner of the web. Comparing with the general observations from monolithic H-walls [22], the precast H-walls exhibited similar failure characteristics with their monolithic counterpart, such as the inclined cracks that developed in the webs and the eventual web crushing. However, due to the associated confinement effect from the encasing steel plates, both the flanges and the web in the precast H-walls maintained in a better condition than the cast-in-situ H-walls.

3.2. Global response analysis

3.2.1 Load-displacement relationship and key points

The lateral load versus top displacement curves of the three specimens are shown in Fig. 10.

Denote the cracking load, yield load, peak load, and failure load as P_{cr}, P_y, P_m, and P_u, and the corresponding displacements as Δ_{cr}, Δ_y, Δ_m, and Δ_u, respectively. The determination of the yield load for situations where there is not a clear yielding plateau, different methods may be used to estimate Δ_y and P_y [23]. In the present study, Δ_y and P_y are determined using the following two methods.

(1) the lateral load and top displacement corresponding to the first yielding of the tension steel farthest from the compression end of the wall panel are taken as yield load (P_y) and yield displacement (Δ_y), respectively.

(2) the yield load (P_y) is firstly calculated as P_y=0.85P_m, and the yield displacement is estimated by extending a line connecting the origin and the point of 0.6P_y on the load-displacement curve to the horizontal line of P=P_y; the displacement of the resulting intersection is assumed as yield displacement (Δ_y).

After the maximum load was reached, the ultimate displacement Δ_u was determined when the lateral load decreased to 85% of the maximum lateral force. The test was terminated upon reaching this point unless it became unstable earlier.

The results of the above key points are summarized in Table 3.

From Table 3 together with Fig. 10 the following observations can be made:

(1) The three specimens reached an average peak lateral load resistance of 669 kN. Comparing with the two preliminary specimens (WV-1 and WV-2), which had similar properties as the current specimens except the framing and connection details, the lateral capacity increased by more than 50%.

This is attributable to the encasing steel plate around the wall web which reinforced the web panel with an effect similar to boundary columns. This is analyzed in detail in the mechanism analysis section.

(2) The measured ultimate drift ratios listed in Table 3 for the three test specimens were all greater than the limiting drift value, 1/120, specified in the Chinese Code for seismic design [24], indicating the deformation capacity of the assembled H-walls is sufficient for practical seismic design.

(3) The cracking drift ratio (Δ_{cr}/H) of specimen WV-r2 was larger than that of specimen WV-r1 by about 76%, this indicates that the initial lateral stiffness of specimen WV-r1 was larger than that of specimen WV-r2. Therefore, it can be inferred that reducing the thickness of the connecting element in specimen WV-r2 relative to WV-r1 reduced noticeably the initial lateral stiffness of the test wall.

(4) The peak load (P_m) of specimen WV-r2 was smaller than that of specimen WV-r1 by about 20%, indicating that reducing the thickness of the connecting element in specimen WV-r2 by a half relative to specimen WV-1 reduced P_m markedly, by approximately 20% herein.

3.2.2 Ductility and energy dissipation

Table 4 compares the experimental ductility of the three test walls with the previous two specimens WV-1 and WV-2 in terms of displacement ductility factor, μ, which is defined as the ratio between the ultimate displacement to the yield displacement, namely $\mu=\Delta_u/\Delta_y$. This table shows that the displacement ductility factors for the improved specimens are about twice those for specimens WV-1 and WV-2, indicating the ductility performance of the modified test walls were significantly improved when compared to the preliminary specimens.

The energy dissipation capacity may be evaluated from cyclic load tests, so this is calculated for the specimen WV-r3 only. In general terms, the energy absorbed by a structural member subjected to

cyclic loading can be evaluated using the area enclosed within hysteretic load-displacement loops. Herein two parameters, namely equivalent energy dissipation ratio E and equivalent viscous damping ratio h_e [25], are adopted to evaluate the energy-dissipating capacity of the specimens.

Figs. 11 (a) and (b) show E and h_e versus top displacement curves for specimen WV-r3 subjected to cyclic loading, respectively. As can be seen: E increased with the increasing lateral displacement. Especially after the yielding, E increased almost linearly with the displacement increment until the test wall failed. Similarly, h_e increased with the increase of the lateral displacement. At first, h_e fluctuated around a level of 4% before the yielding, while after the yielding it increased almost linearly with the displacement increment to reach about 15.2% when specimen failed. The average hysteretic damping ratio was close to 10%, indicating a good energy-dissipating capacity. When the H-walls reached peak point and failure point, the energy-dissipating capacity of the modified H-walls was on average 116% larger than the preliminary walls in terms of the two ratios.

3.3. Performance analysis of bolted steel connections

3.3.1 Effectiveness of vertical bolted connections

Based on the measured strains in vertical steel bars, Fig. 12 shows schematically the strain distribution on the bottom section of the specimens subjected to monotonic loading. In the figures, the horizontal coordinates of 0 and 100 stand for the tension and compression ends of the specimens, respectively. It can be seen that the strains distribution in the vertical steel bars at the specimen bottom was nearly linear at each loading stage. This result demonstrates the vertical bolted connections in the test walls worked effectively. It also confirmed that the plane cross-section remaining plane may be applied in the analysis of the type of walls.

Furthermore, during each test the tensile flange bottom firstly cracked and expanded, the wall

web then cracked and the cracks extended gradually to the compression corner. When the specimens failed, the crack penetrated through the tensile flange bottom; meanwhile the concrete crushed at the web compression corner and compressive flange bottom. These features indicate that the flange and the web of the H-wall behaved in a manner of a composite section.

The effectiveness of vertical bolted connections can be further examined according to the strain measurement and analysis results, as discussed in the next section.

3.3.2 Strain in the connecting steel frame

The vertical connections in the H-shaped shear wall serve to join the adjacent longitudinal and transverse walls (that is, flange and web, respectively) together through shear transfer between the flange and web walls [25] to ensure the whole unit acts as an entirety to resist the lateral loading. Therefore, during the monotonic tests some strain rosettes, as mentioned in Section 2.3.2, were installed on CSF web and flange to measure the strain state. For the sake of convenience, each part in the specimen is named as shown in Fig. 13.

The shear strain distribution along the vertical component in the CSF is instructive for the analysis of the integrity of the H-wall assembly. The shear strain can be calculated from the measured data of the strain rosettes. Fig. 14 and 15 show the vertical shear strain in CSF web versus top displacement for specimens WV-r1 and WV-r2, respectively. It can be observed from these figures that:

(1) On the compression side, the shear strains in the bottom part of CSF web (e.g. No. 17 in Fig. 14 (a)) were larger than those in the upper part of CSF web (e.g. No. 18 - 23 in the same figure) especially when the specimens failed. It can be inferred that the CSF bottom transferred the main shear force on the compressive side of the H-wall.

(2) On the tension side, the shear strains in the top part of CSF web (e.g. No. 9 and 11 in Fig. 15 (b)) were significantly larger than those in the bottom part of CSF web (e.g. No. 1 and 3 in the same figure), indicating that the upper CSF transferred a large part of the vertical shear force on the tensile side.

(3) The strains in CSF in specimen WV-r2 were almost twice as larger as those of specimens WV-r1; this should be attributable to the fact that the CSF thickness t in WV-r2 (3 mm) was only half that in WV-r1 (6 mm).

3.3.3 Relative displacement (sliding) within connections

Ggenerally the bolted steel connection successively experienced friction phase, sliding phase, and bearing phase as the lateral displacement increased. At the friction phase, the internal forces between the assembled wall panels were transferred in the connections through the friction action on the surface within the bolted connection; when the friction force was overcome, sliding occurred until the bolts came into contact with the wall of bolt holes, and bearing took over afterwards. During the bearing phase, the force transfer was mainly achieved by the bearing action between the bolts and wall of bolt holes. The relative displacement (sliding) within the vertical bolted connections were measured throughout the test.

The following observations can be made from the measured data: 1) there was no global sliding on neither tensile nor compressive sides; 2) the sliding within the connection at the tensile zone of the web had a maximum sliding of about 1.13 mm, and it was evidently larger than those at the compressive zone of the web, where a maximum sliding of about 0.66 mm was measured.

4. Ultimate lateral load - resistance mechanism

4.1. Basic assumptions and shear-resistance model

As mentioned in the beginning, the preliminary specimens WV-1 and WV-2 (under cyclic lateral loading) eventually failed due in a shear failure mode, resulting in a poor seismic behavior and a very limited ductility performance of the whole H-shaped wall assembly. The experiment in the present study improved the details of the vertical bolted connection, and the test results showed that the seismic behavior of the modified precast H-wall significantly improved in terms of the loading bearing capacity, ductility, and energy dissipation capacity. This section presents a conceptual analysis of the shear-resistance mechanism of the modified H-wall under ultimate limit state.

The following assumptions are adopted to analyze the ultimate shear-resistance mechanism of the modified walls:

(1) When the H-wall developed into ultimate limit state, the shear-resistance mechanism of the H-wall consists of the diagonal compression concrete struts (I), the pull rods formed from the vertical distributing steel in the web (II), the tensile and compressive flanges (III and IV), the pull and push rods formed from the vertical ESP on the tensile and compressive sides of the web (V and VI), respectively, and the ESP at the top of web (VII). The last three components (V, VI, and VII) are the distinctive features of the current design of the H-wall assembly.

(2) Both the longitudinal steel in the tensile flange and the vertical distributing steel within the tensile zone of web yielded under tension and the vertical distributing steel within the compressive zone of the wall web yielded as well under compression.

On the above basis, the ultimate anti-shearing mechanism for the modified H-shaped shear wall assembly can be illustrated as shown in Fig. 16 (a). For comparison purposes, the ultimate

shear-resistance mechanism for the preliminary test walls is presented in Fig. 16 (b).

4.2. Discussion on shear-resistance mechanism

From the shear-resistance mechanism of the modified H-wall together with Fig. 16 the following observations can be made:

(1) The lower end of the diagonal compression concrete struts (I) transferred a large part of the interactional force between web and flange, therefore it can be predicted that the CSF in this area is susceptible to buckling if the thickness of CSF reduces to below a certain limit. According to the experimental results for specimen WV-r2, a reduction of the thickness from 6 mm to 3 mm caused buckling.

(2) It can be deduced that after the diagonal compression concrete struts (I) degraded due to the crushing of concrete at the lower corner, the pull rod (V), push rod (VI) together with the ESP (VII) at the web top could postpone the reduction of the lateral load and increase the ductility performance of the precast H-walls.

Furthermore, the comparison of the anti-shearing mechanisms between the current specimens (WV-r1 through WV-r3) and the preliminary test walls (WV-1 and WV-2) shows the following:

(1) The ESP serves as pull and push rods when the modified H-walls were subjected to lateral load, which makes great contribution to the flexural bearing capacity of the improved walls.

(2) The lower end of the ESP at compressive side of web can bear horizontal shear force, which constitutes a component of the shear bearing capacity of the improved H-walls.

In summary, in consideration of the concurrence of vertical and horizontal connections in practical structure, the added horizontal and vertical encasing steel plates (ESP) around the concrete wall effectively enhanced both the shear bearing capacity and the flexural bearing capacity of the

precast shear wall assembly, as well as the ductility performance of the H-wall.

5. Conclusions

This paper presents an experimental study on the lateral load behaviour of an H-shaped precast shear wall design with vertical connections. Three specimens were tested to failure under lateral load while subjected to constant axial (vertical) compression. Based on the experimental results and mechanism analysis, the following conclusions may be drawn:

(1) The general idea of assembling precast RC wall through vertical bolted steel connections was workable in terms of both the assembling procedure and the anticipated effect. The connecting steel frame (CSF) and bolts can effectively connect the longitudinal and transverse precast RC wall panels and transfer the interactional forces between them, such that the two directional walls work together as an integrated H-wall to resist the lateral load.

(2) The H-walls assembled vertically using bolted steel connections exhibited satisfactory seismic behavior in terms of lateral load bearing capacity, ductility performance and energy dissipation. The ultimate load bearing capacity of the current design was roughly 50% greater that of the preliminary specimens (WV-1 and WV-2). The displacement ductility factors for the improved H-walls were in a range of 3.2 to 5.4, about twice the values achieved in the preliminary specimens.

(3) The modified connection detailing proved favourable for the energy dissipation of the H-walls. When the H-walls reached peak point and failure point, the energy-dissipating capacity of the modified H-walls was on average 116% larger than the preliminary walls.

(4) The thickness (t) of the steel plate contained in the connecting steel frame (CSF), influenced both the lateral stiffness and the ultimate load bearing capacity of the H-walls. It was shown that when t reduces from 6 mm to 3 mm, the connecting steel frame (CSF) will buckle prior to the crushing of

concrete in compressive zone.

(5) The encasing steel plates (ESP) around the precast RC wall not only helped transfer the stress among the wall reinforcement, but also acted as the reinforcement in the web boundary column as well as confines the concrete there, leading to favorable ductility and high load bearing capacity of the precast RC H-wall.

Acknowledgements

The authors are grateful for the financial support provided by Jiangsu Natural Science Foundation (No. BK20170668), National Natural Science Foundation of China (No. 51708107), and the Fundamental Research Funds for the Central Universities.

References

[1] D. C. Feng, Z. Wang, G. Wu, Struct. Des. Tall Spec. Build. 2019, 28(5), e1588.

[2] R. E. Englekirk, Struct. Des. Tall Spec. Build. 2004, 13(5), 457.

[3] Y. C. Kurama, S. Sritharan, R. B. Fleischman, J. I. Restrepo, R. S. Henry, N. M. Cleland, S. K. Ghosh, P. Bonelli, J. Struct. Eng. 2018, 144(4), 03118001.

[4] X. Ren, Q. Bai, C. Yang, J. Li, Struct. Des. Tall Spec. Build. 2018, 27(4), e1441.

[5] G. V. Rama Rao, N. Gopalakrishnan, K. P. Jaya, K. Muthumani, G. R. Reddy, Y. M. Parulekar, J. Perform. Constr. Facil. 2016, 30(1), 04014201.

[6] Y. Kurama, S. Pessiki, R. Sause, L. Lu, PCI J. 1999, 44(3), 72.

[7] F. J. Perez, R. Sause, S. Pessiki, J. Struct. Eng. 2007, 133(11), 1531.

[8] R. S. Henry, N. J. Brooke, S. Sritharan, J. M. Ingham, ACI Struct. J. 2012, 109(1), 101.

[9] F. J. Perez, S. Pessiki, R. Sause, ACI Struct. J. 2013, 110(6), 1045.

[10] Y. C. Kurama, PCI J. 2002, 47(5), 36.

[11] B. J. Smith, Y. C. Kurama, M. J. McGinnis, J. Struct. Eng. 2013, 139(11), 1917.

[12] A. Belleri, M. J. Schoettler, J. I. Restrepo, R. B. Fleischman, ACI Struct. J. 2014, 111(3), 661.

[13] M. Shemie, PCI J. 1973, 18(1), 27.

[14] A.S. Pall, C. Marsh, P. Fazio, PCI J. 1980, 25(6), 38.

[15] O. A. Pekau, D. Hum, PCI J. 1991, 36(2), 56.

[16] C. Bora, M. G. Oliva, S. D. Nakaki, R. Becker, PCI J. 2007, 52(1), 122.

[17] W. Lim, T. H. Kang, S. Hong, ACI Struct. J. 2016, 113(1), 179.

[18] J. Sun, H. X. Qiu, H. B. Jiang, Struct. Concr. 2019, 20(1), 282.

[19] J. Sun, H. X. Qiu, J. P. Xu, Adv. Struct. Eng. 2015, 18(7), 1071.

[20] J. Sun, H. X. Qiu, J. Cent. South Univ. 2015, 22(4), 1536.

[21] MOHURD (Ministry of Housing and Urban-Rural Development of the People's Republic of China). Technical specification for high strength bolt connections of steel structures. JGJ 82-2011, Beijing. 2011.

[22] R. G. Oesterle, J. D. Aristizabalochoa, K. N. Shiu, W. G. Corley, ACI Struct. J. 1984, 81(3), 231.

[23] R. Park, Bull. N. Z. Natl. Soc. Earthq. Eng. 1989, 22(3), 155.

[24] MOHURD (Ministry of Housing and Urban-Rural Development of the People's Republic of China). Code for seismic design of buildings. GB50011-2010, Beijing. 2010.

[25] Y. Z. Fang, C. D. Lu, J. Ma, L. Shen, G. H. Sun, China Civ. Eng. J. 2013, 46(1), 24. [in Chinese]

Table 1 Measured material properties

Material	f_y (MPa)	f_u (MPa)
HPB300A6 steel bar	362	530
HPB300A8 steel bar	370	583
3-mm-thick steel plate	296	350
6-mm-thick steel plate	350	441

Table 2 Loading schemes

Specimen	Loading scheme	Loading method
WV-r1	At the early stage, lateral loading was applied in a force-controlled manner and the load step interval was set at 20 kN until the specimen yielded; the loading was then applied in a displacement-controlled manner and the displacement step interval was set at 5 mm until the specimen failed.	Monotonic
WV-r2	Lateral loading was applied in a displacement-controlled manner throughout the test. At the early stage, the displacement step interval was set at 1 mm until the top displacement reached 12 mm; top displacement was then increased to 15 mm; after that the step interval was further increased to 5 mm until the specimen failed.	Monotonic
WV-r3	Similar displaced controlled loading as WV-r2 but in cyclic manner as shown in Fig. 5.	Cyclic

Table 3 Performance indexes of specimens

Specimens	Loading direction	Cracking point			Yield point						Peak point			Failure point		
					(1)			(2)								
		P_{cr}	Δ_{cr}	Δ_{cr}/H	P_y	Δ_y	Δ_y/H	P_y	Δ_y	Δ_y/H	P_m	Δ_m	Δ_m/H	P_u	Δ_u	Δ_u/H
WV-r1	Push	180	3.4	1/684	430	14.0	1/166	613	19.4	1/120	721	44.8	1/52	621	75.0	1/31
WV-r2	Push	211	6.0	1/388	362	15.0	1/156	492	18.8	1/128	579	49.0	1/48	511	69.6	1/33
WV-r3	Push	185	4.0	1/582	414	12.0	1/194	642	17.9	1/131	755	39.6	1/59	642	56.2	1/41
	Pull	163	4.0	1/582	350	12.0	1/195	561	18.7	1/124	660	55.0	1/42	593	60.1	1/39

Note: H is the wall height measuring from the loading point to the concrete wall bottom; the units of the loads and displacements in this table are kN and mm, respectively.

Table 4 Displacement ductility factor

Methods	Previous specimens [19]				Improved specimens			
	WV-1		WV-2		WV-r1	WV-r2	WV-r3	
	Push	Pull	Push	Pull			Push	Pull
Method (1)	2.1	2.2	2.1	2.0	5.4	4.7	5.0	5.0
Method (2)	2.3	2.3	2.5	2.4	3.9	3.8	3.4	3.2

Captions of figures

Fig. 1 Preliminary specimens WV-1 & WV-2 and ultimate failure mode [19]: (a) Wall configuration and (b) Typical failure mode

Fig. 2 New design of precast H-wall specimens: (a) Configuration of new H-wall specimens and (b) Details of separate units of the specimens

Fig. 3 Assemblage of the precast RC H-wall: (a) Assembling of web and flanges and (b) Finished H-wall unit

Fig. 4 Test setup: (a) Front view of schematic, (b) Lateral view of schematic, and (c) Photograph

Fig. 5 Load protocol for cyclic test (WV-r3)

Fig. 6 Measurement scheme: (a) Layouts of strain gauges and LVDTs and (b) Strain gauges on vertical steel bars on Section 6−6

Fig. 7 Crack pattern and failure mode for WV-r1: (a) First bending crack, (b) Web inclined cracks, (c) Crushing of concrete, (d) General failure mode, and (e) Crack distribution in the web panel

Fig. 8 Crack pattern and failure mode for WV-r2: (a) First bending crack, (b) Web inclined cracks, (c) Crushing of concrete, (d) Local buckling, (e) General failure mode, and (f) Crack distribution in the web panel

Fig. 9 Crack pattern and failure mode for WV-r3: (a) Crushing of concrete, (b) General failure mode, (c) Crack distribution in the web panel

Fig. 10 Load-displacement curves: (a) Monotonic tests for WV-r1 and WV-r2 and (b) Cyclic test for WV-r3

Fig. 11 E and h_e for specimen WV-r3: (a) Equivalent energy dissipation ratio and (b) Equivalent

viscous damping ratio

Fig. 12 Strain distribution at bottom section of test walls: (a) Specimen WV-r1 and (b) Specimen WV-r2

Fig. 13 Designation of each part in the H-wall assembly

Fig. 14 CSF shear strain distribution in WV-r1: (a) CSF web on compressive side and (b) CSF web on tensile side

Fig. 15 CSF shear strain distribution in WV-r2: (a) CSF web on compressive side and (b) CSF web on tensile side

Fig. 16 Ultimate shear-resistance mechanism: (a) Improved specimens and (b) Preliminary specimens WV-1 and WV-2 [20]

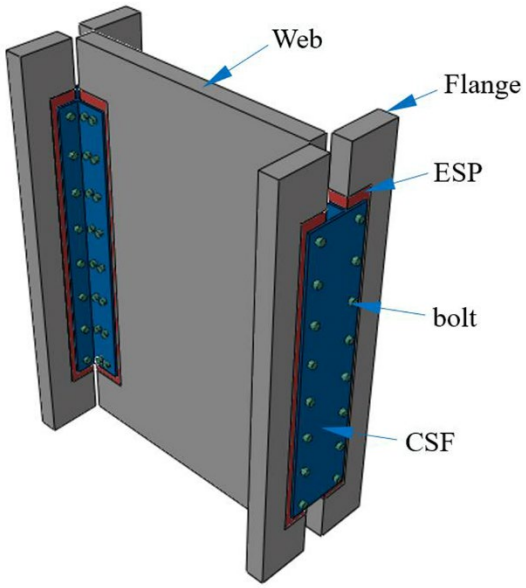

Fig. 1(a)

Fig. 1(b)

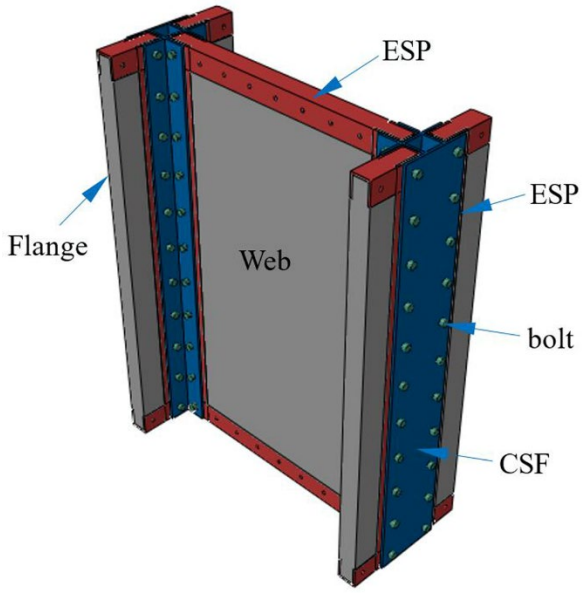
ESP
ESP
Flange
Web
bolt
CSF

Fig. 2(a)

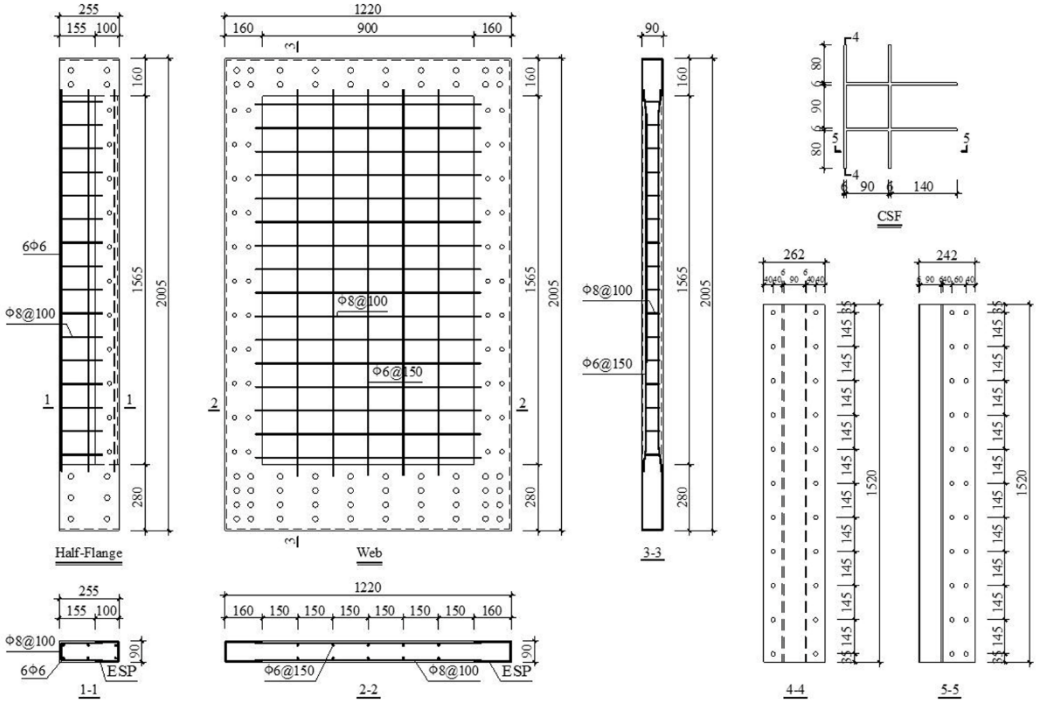
Half-Flange
Web
3-3
CSF
1-1
2-2
4-4
5-5
ESP
ESP

Fig. 2(b)

Fig. 3(a)

Fig. 3(b)

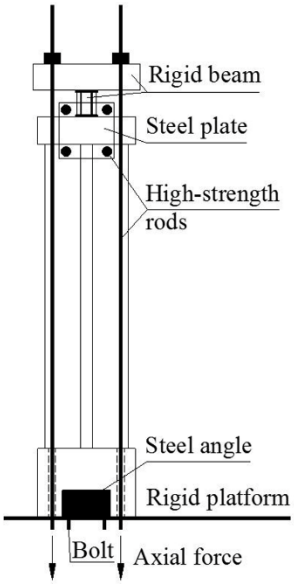

Fig. 4(a)

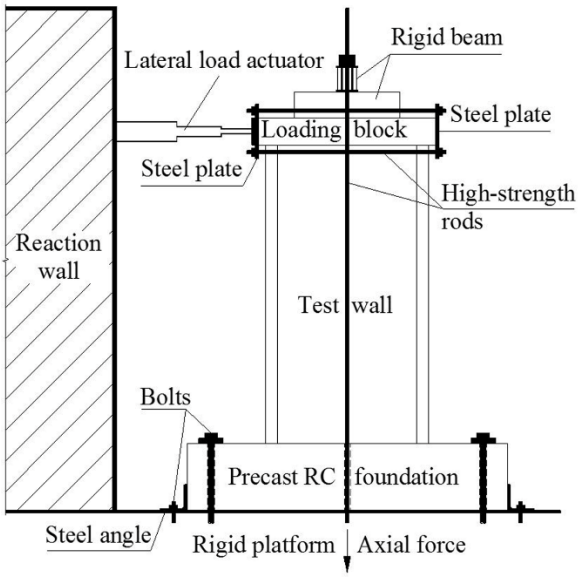

Fig. 4(b)

Fig. 4(c)

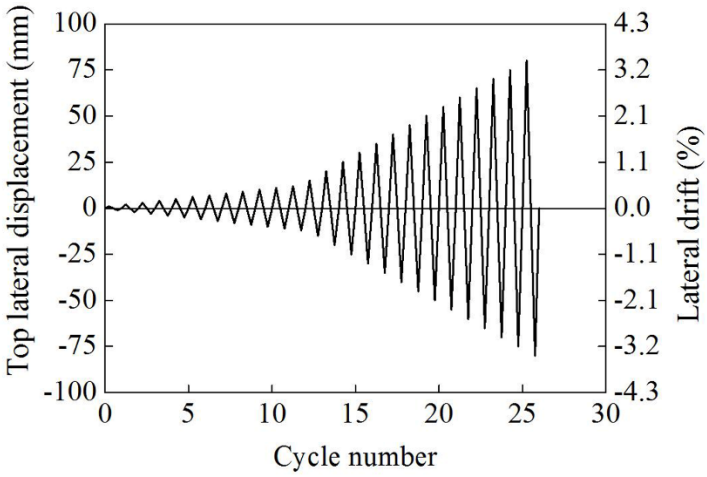

Fig. 5

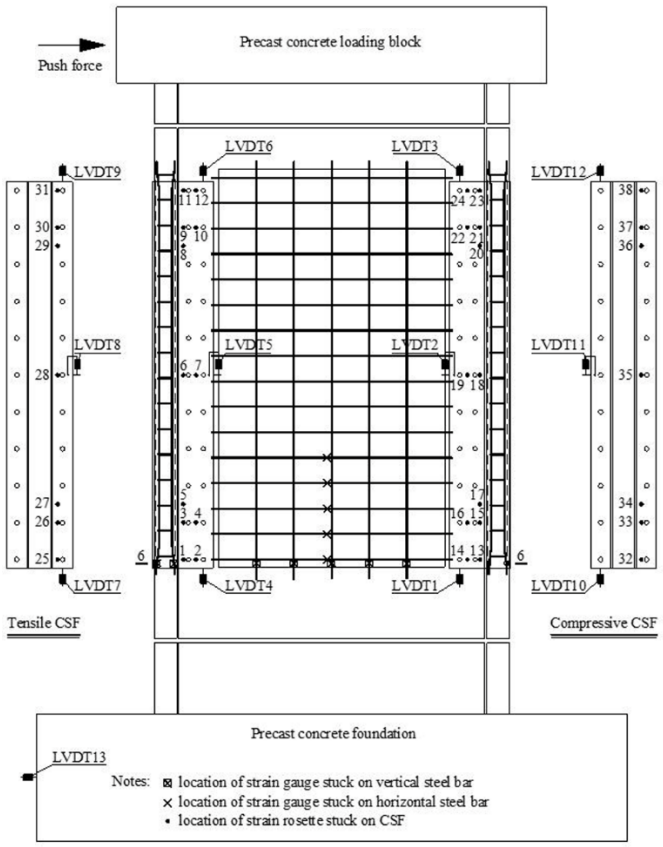
Precast concrete loading block
Push force
LVDT6
LVDT3
LVDT9
LVDT12
LVDT8
LVDT5
LVDT2
LVDT11
LVDT7
LVDT4
LVDT1
LVDT10
Tensile CSF
Compressive CSF
Precast concrete foundation
LVDT13
Notes: location of strain gauge stuck on vertical steel bar
location of strain gauge stuck on horizontal steel bar
location of strain rosette stuck on CSF

Fig. 6(a)

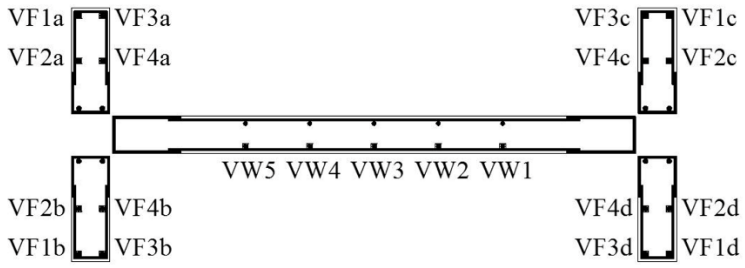
VF1a
VF3a
VF2a
VF4a
VF3c
VF1c
VF4c
VF2c
VW5 VW4 VW3 VW2 VW1
VF2b
VF4b
VF1b
VF3b
VF4d
VF2d
VF3d
VF1d

Fig. 6(b)

Fig. 7(a)

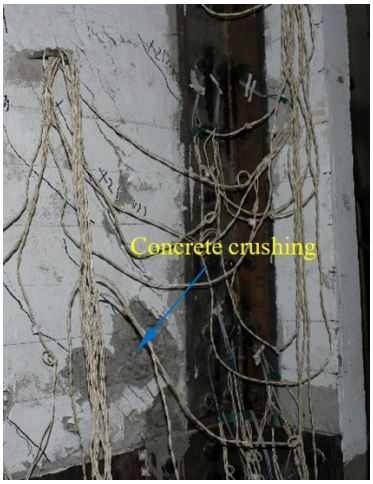

Fig. 7(b)

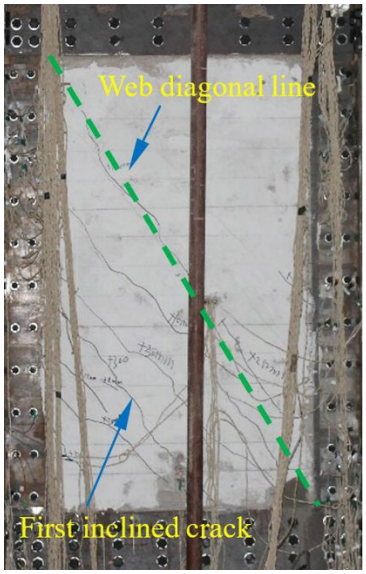

Fig. 7(c)

Fig. 7(d)

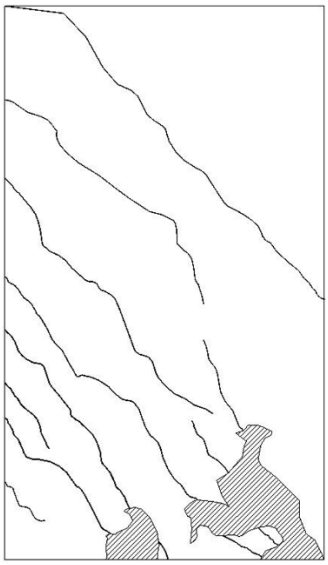

Fig. 7(e)

Fig. 8(a)

Fig. 8(b)

Fig. 8(c)

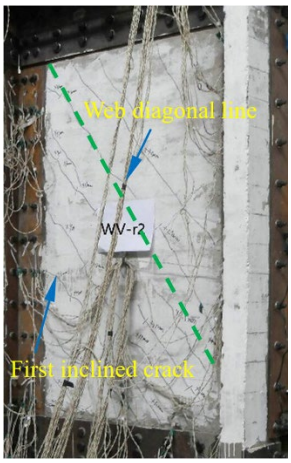

Fig. 8(d)

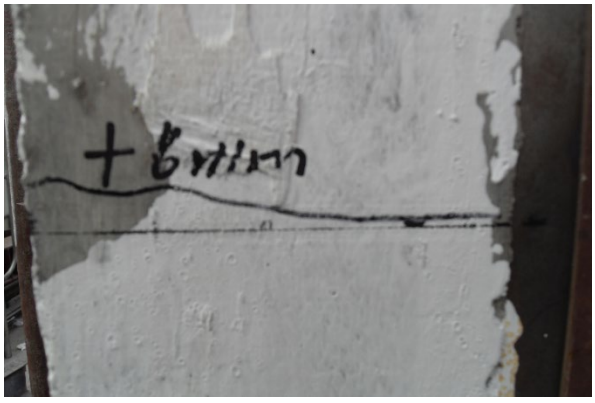

Fig. 8(e)

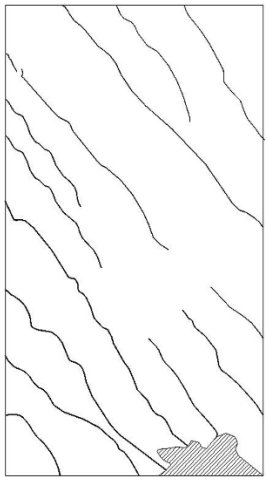

Fig. 8(f)

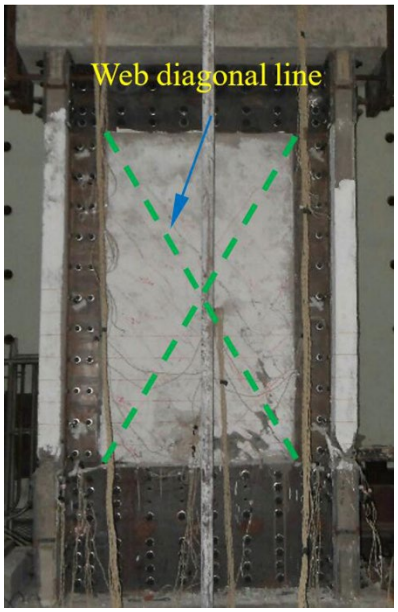

Fig. 9(a)

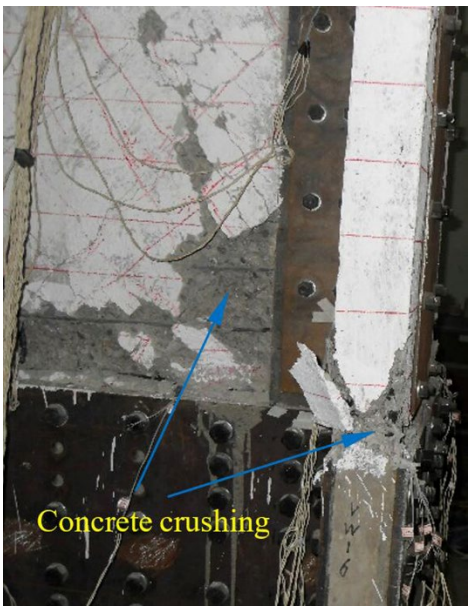

Fig. 9(b)

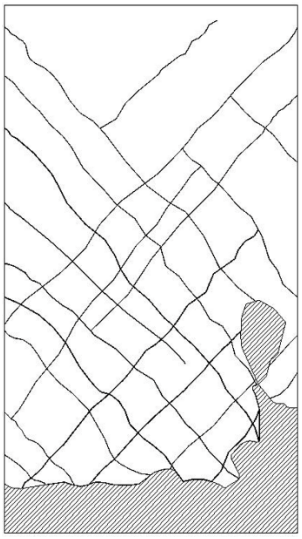

Fig. 9(c)

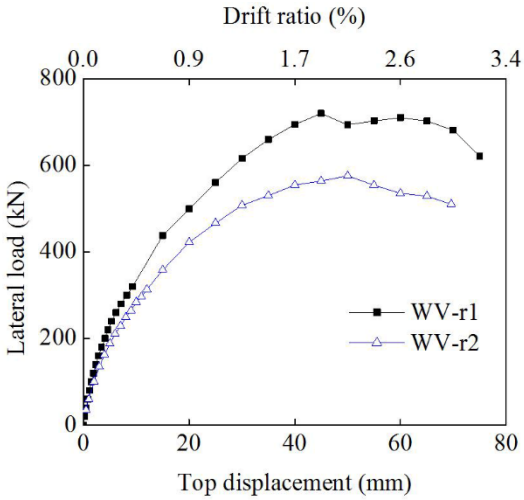

Fig. 10(a)

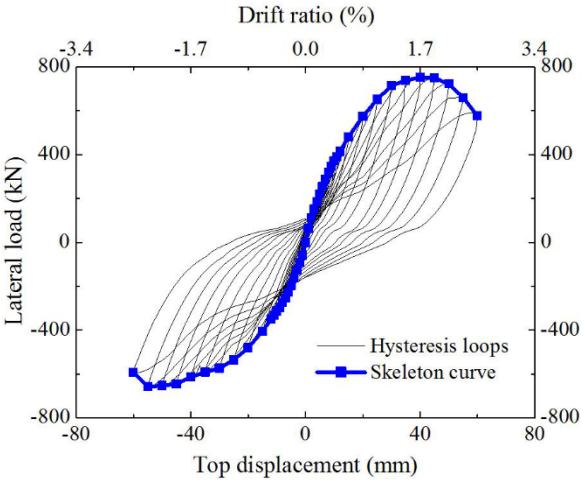

Fig. 10(b)

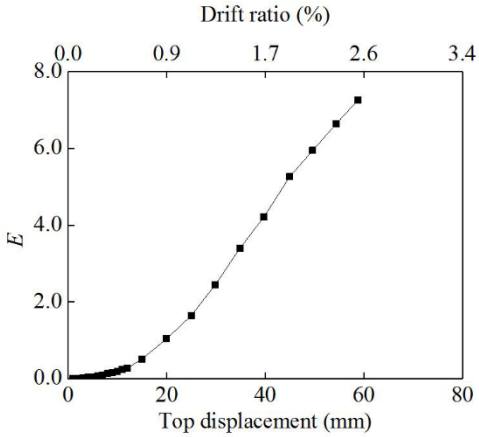

Fig. 11(a)

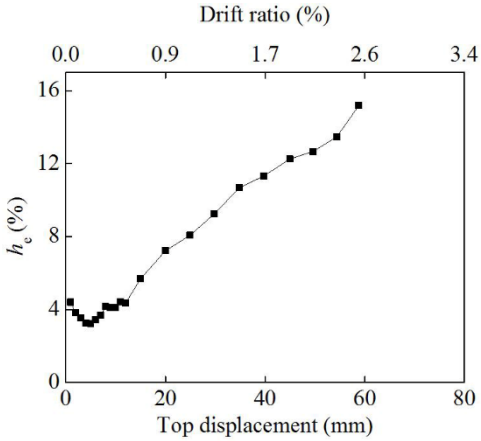

Fig. 11(b)

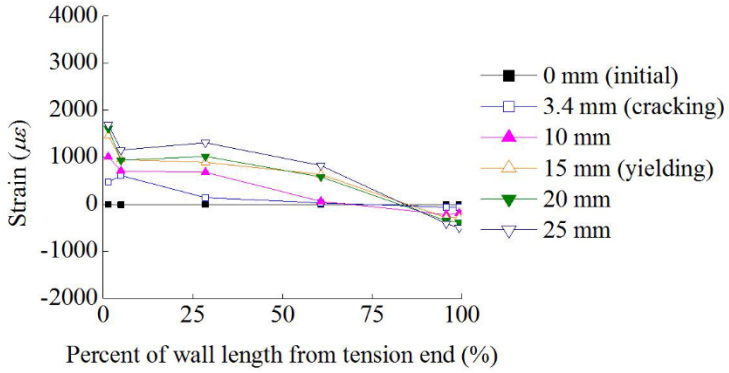

Fig. 12(a)

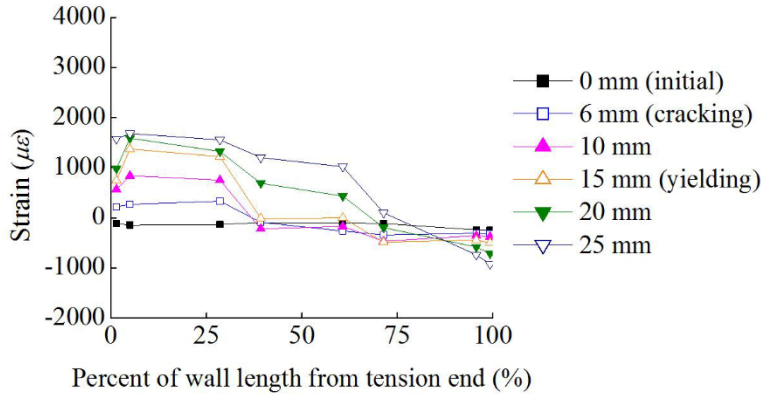

Fig. 12(b)

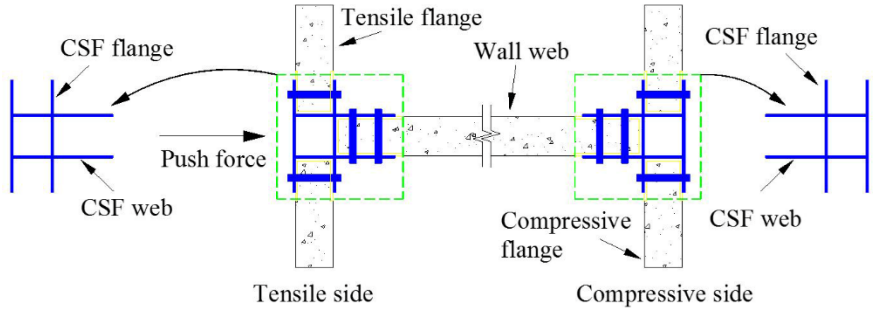

Fig. 13

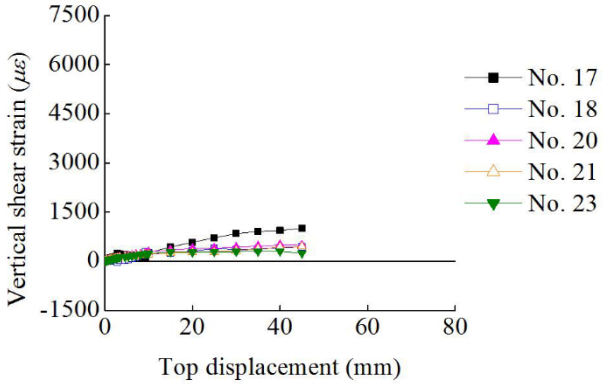

Fig. 14(a)

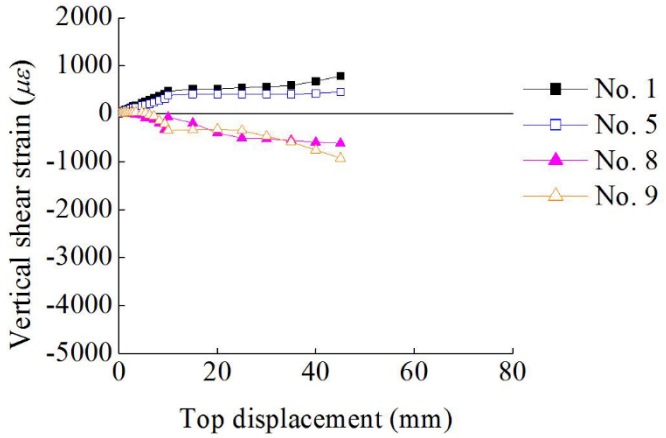

Fig. 14(b)

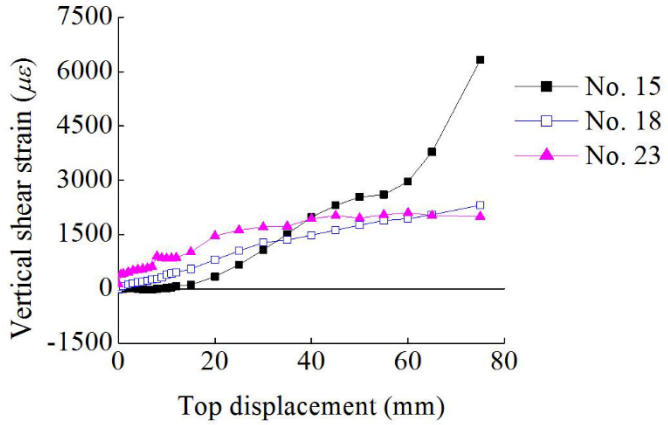

Fig. 15(a)

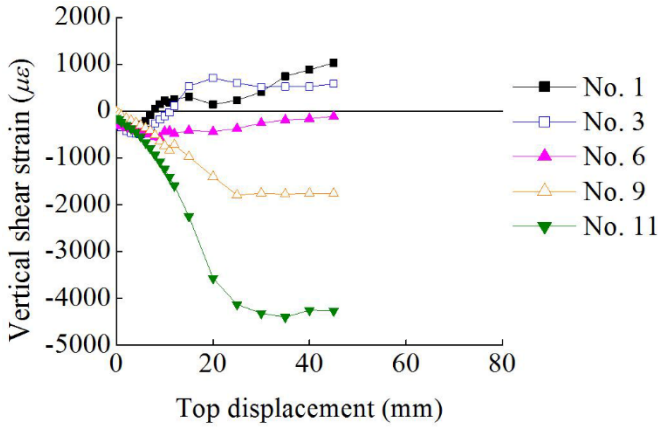

Fig. 15(b)

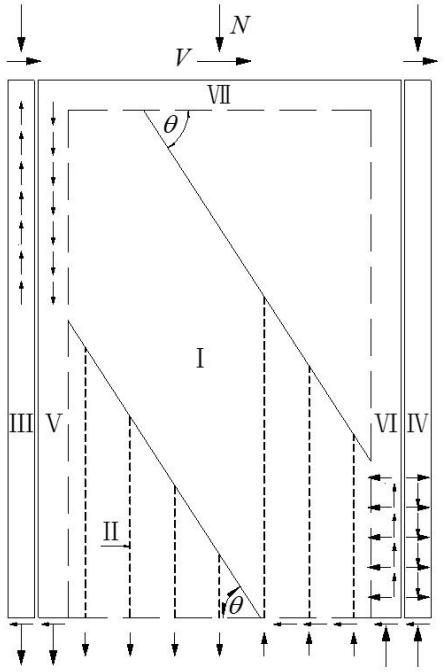

I — diagonal compression concrete struts
II —pull rods formed from the vertical distributing steel in wall web
III and IV—tensile and compressive flange
V and VI—pull and push rods formed from the vertical ESP on the tensile and compressive sides of the wall web
VII—ESP at the top of wall web

Fig. 16(a)

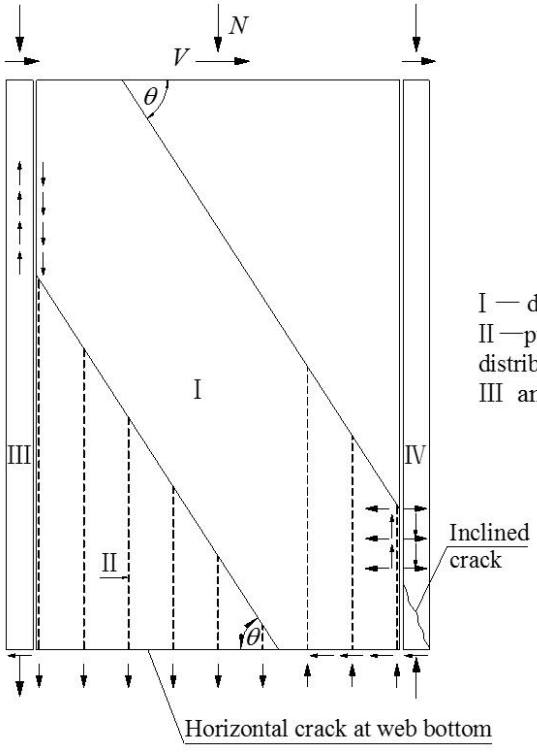

I — diagonal compression concrete struts
II —pull rods formed from the vertical distributing steel in wall web
III and IV—tensile and compressive flange

Fig. 16(b)